Insights into orogenic processes from drab schists and minor intrusions: Southern São Francisco Craton, Brazil

Hugo Moreira[a], Lucas Cassino[b], Cristiano Lana[b], Craig Storey[a], Capucine Albert[b,c]

[a] School of Earth and Environmental Sciences, University of Portsmouth, Burnaby Building, Burnaby road, Portsmouth, PO1 3QL, UK;

[b] Applied Isotope Research Group, Departamento de Geologia, Escola de Minas, Universidade Federal de Ouro Preto, Ouro Preto, MG 35400-000, Brazil;

[c] Department of Earth Sciences, University of Cambridge, Downing Street, Cambridge CB2 3EQ, UK

Supplementary material

Additional description

Two thin-sections were imaged at high resolution using a Scanning Electron Microscope SEM (Zeiss EVO MA 10 LaB6 SEM) at the University of Portsmouth, UK. A silicon drift (SDD) Oxford X-max 80 mm^2 detector attached to the SEM was used for Energy Dispersive X-ray Spectroscopy (EDS) to determine the mineral phases and to produce element compositional maps; EHT voltage of 20 kV and beam current of 500 pA were used and the resolution was 2048 $pixels^2$ with dwell time varying from 20 µs to 100 µs. Averaging counts were 60 Kcps.

Sample B1a is composed essentially by quartz (ca. 40%), epidote (ca. 25%), chlorite (ca. 30%) and accessory phases (ca. 5%) are magnetite, ilmenite, rutile and zircon. The sample is intensively deformed marked by main foliation and cleavage. Titanite is not present, but rutile is common, range in size from a few microns to half mm and is generally porous and partially dissolved, although sub-euhedral grains can be found (Fig 1 supplementary). Zircon grains appear to be relict related to the main schistosity and inclusions are rare (Fig 2 supplementary). Ilmenite is found as relict cores rimmed by rutile (Fig 3 supplementary). Tourmaline was not identified in thin-section but is abundant in the heavy concentration after panning. Noticeable, picked rutile grains from the heavy concentration material are largely more abundant as a pristine population than the porous counterpart. Yet, it is possible to visualize dissolution features and ilmenite inclusions in the picked grains, which suggests they share the same origin. This is due to the tendency of highly porous grains get pulverized during comminution procedure. Inclusions in magnetite were also identified in order to try to find any other evidence of high-grade metamorphism as the potential garnets could have retrogressed to magnetite. Inclusions are mostly quartz, epidote and rutile. The latter is texturally similar to the matrix counterpart but smaller (up to 20 μm in length).

Intrusion B2a from this locality is relatively fresher and thin-sections were produced. They show granolepidoblastic texture formed by plagioclase (ca. 50%) up to 5 mm in length and quartz (ca. 30%) crystals surrounded by phyllosilicates (Fig 4 supplementary). Greenschist metamorphic facies after retrogression is evident by largely amount of chlorite (ca. 15%) and also the presence of K-feldspar, epidote and muscovite recrystallized within the plagioclase. Epidote is also present in the matrix and along with biotite, primary muscovite, rutile and zircon compose 5% of the sample. Rutile grains compose a trail that follows the main foliation, possibly caused by dissolution and recrystallisation (Fig 5 supplementary). Textural similarities between the rutile grains from sample B1a and B2a suggest they were formed at the same time. The two-mica paragenesis and lack of evidence for remobilization of the melt suggest a low grade anataxis of local sediments as the precursor of these rocks. The presence of tourmaline in the host reinforces this hypothesis as boron can lower substantially the melting point of anatectic melts. The presence of fluids are likely to have assisted melt at relatively lower temperature of these sediments during the Palaeoproterozoic.

Description of supplementary figures

Figure 1: SEM-EDS elemental mapping of thin-section from schist B1a and Backscatter-electron (BSE) image of the same mapped area. Main mineral phases are indicated.

Figure 2: BSE image of a zircon grain from sample B1a and main mineral phases associated.

Figure 3: EDS mapping of relict unstable ilmenite reacting to porous rutile. Other mineral phases also shown. BSE of the same area also presented.

Figure 4: Thin-section of sample B2a. The felsic intrusion is mostly composed by albite, quartz and chlorite. Biotite, rutile, epidote and primary white-mica are also present. BSE image of the same area also shown. Note the porosity within the rutile grains, similar to those from sample B1a.

Figure 5: Thin-section of coarser part of intrusion B2a mostly composed by plagioclase and quartz. Note the presence of epidote and secondary mica within the albite. Chlorite is the main phyllosilicate in the section. BSE image also presented.

Figure 6: Concordia diagram of U-Pb rutile analyses after common lead correction based on ^{208}Pb. The oldest rutile grains are not 100% concordant, but are Archaean in age. Most of grains were reset during the Palaeoproterozoic.

Additional images

A) Optical microphotographs of rutile grain with two distinct ages suggesting resetting of the U-Pb system. Zirconium concentration is very similar because it diffuses slower than Pb and likely represent Archaean crystallisation temperature; **B)** Heavy minerals from sample B1a. Presence of rutile, zircon and tourmaline; **C)** Optical microscope stage rotated at 90° compared to previous picture. Note the characteristic reverse pleochroism in tourmaline grain; **D)** Possible porosity in rutile after recrystallisation; **E)** Relict ilmenite within rutile; **F)** Transparent and predominantly pale-pink colour soccer ball zircon grains; **H)** Cathodoluminescence of soccer ball zircons shown in figure F.

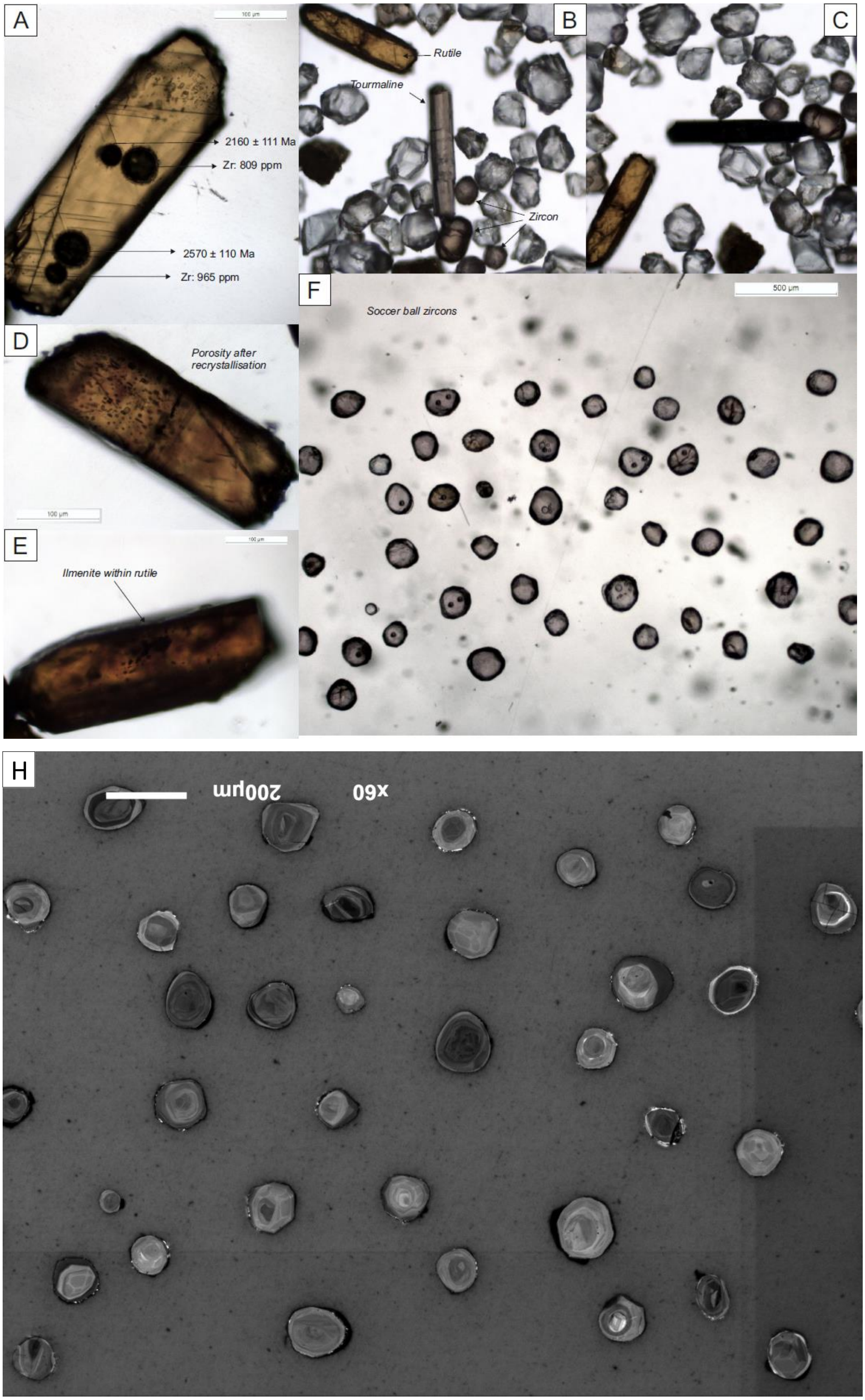
A
100 µm
2160 ± 111 Ma
Zr: 809 ppm
2570 ± 110 Ma
Zr: 965 ppm
B
Rutile
Tourmaline
Zircon
C
D
Porosity after recrystallisation
100 µm
E
Ilmenite within rutile
100 µm
F
Soccer ball zircons
500 µm
H
200µm
x60